Geochemical Study of Detrital Apatite in Sediment from the Southern Okinawa Trough: New Insights into Sediment Provenance

Siyi Hu [1,2], Zhigang Zeng [1,2,3,*], Xue Fang [1,2], Haiyan Qi [1], Xuebo Yin [1], Zuxing Chen [1], Xiaohui Li [1] and Bowen Zhu [1,2]

[1] Key Laboratory of Marine Geology and Environment, Institute of Oceanology, Chinese Academy of Sciences, Qingdao 266071, China; husiyi15@mails.ucas.ac.cn (S.H.); fxue13@163.com (X.F.); qihaiyan@qdio.ac.cn (H.Q.); Re_hero@163.com (X.Y.); chenzuxing14@mails.ucas.ac.cn (Z.C.); xiaohuili0526@foxmail.com (X.L.); zhubowen16@mails.ucas.ac.cn (B.Z.)

[2] College of Earth and Planetary Sciences, University of Chinese Academy of Sciences, Beijing 100049, China

[3] Laboratory for Marine Mineral Resources, Qingdao National Laboratory for Marine Science and Technology, Qingdao 266071, China

* Correspondence: zgzeng@ms.qdio.ac.cn

check for updates

Abstract: Detrital apatite is a promising accessory mineral for reliable fingerprinting of the protolith composition of detrital sediment. Here, we present the geochemical compositions of detrital apatites from four sections of a high-resolution (~140 cm/kyr) sedimentary archive from the southern Okinawa Trough (SOT) for constraining sediment source rock types and establishing changes in provenance. a series of diagrams based on the geochemical data show that apatites in Section 1 derived mainly from mafic/intermediate rocks, while apatites in the three younger sections largely originated from mafic/intermediate rocks and acid rocks. Further, the four sections included a few contributions of apatites from alkaline rocks and metamorphic rocks. Through a comprehensive analysis of controlling factors and regional stratigraphy in the study area, we concluded that sediments in the SOT are the weathering/erosion products of sedimentary and meta-sedimentary rocks in the western and northeastern Taiwan Island, with ultimate sources containing a wide variety of rock types. The sediment from rivers in eastern Taiwan did not significantly contribute to deposition in the SOT. Apatites in Sections 2–4 showed strong geochemical similarity but differed from those in Section 1, indicating that the types of weathered/eroded sedimentary rocks in the weathering profile of river drainage basins of Taiwan Island changed in Section 2 (2010–1940 cal. yr BP) and have remained stable since then.

Keywords: detrital apatite; sediment provenance; geochemical composition; the southern Okinawa Trough

1. Introduction

The mineralogical and geochemical characteristics of sedimentary archives from lakes, deltas, and marginal seas have long been used for studying the source-to-sink pathways of terrigenous sediments in response to variations in climate and environment in the geological past [1–6]. However, the bulk composition of sediment is controlled by a complex interplay of many factors, including bedrock composition in the source area, intensity of chemical weathering, grain size of the sediment, transport mechanism, diagenesis, and anthropogenic activity [7,8]. The muddy and sandy sediments resulting from hydrodynamic sorting by tidal and ocean currents generally have different compositions even when derived from the same source under the same conditions, which usually leads to geochemical

trends that are not driven by the variability of sediment provenance [3]. Clay minerals are sensitive indicators that constrain sediment source [4,9–12], and they can be delivered over long distances even under weak water power. Clay mineral composition can only be used to constrain the sediment source of the specified site [12,13], and the mixture of clay minerals from multiple sources may result in problematic interpretation. The original provenance signals may be obscured or overprinted during sedimentary processes [14–18]; thus, revealing sediment provenance using mixed compositions is not straightforward. In recent studies, the geochemical analysis of heavy minerals such as apatite, garnet, rutile, clinopyroxene, zircon, and magnetite has provided much better constraints on sediment provenance, since their varietal characteristics are mainly inherited from source rocks and their compositions are specific to certain parageneses [8,14,18–23]. Among these heavy minerals, detrital apatite is a promising candidate for fingerprinting changes in sediment provenance, mainly because (1) apatite is a common accessory mineral in most igneous, metamorphic, and sedimentary rocks [20,24–26]; (2) apatite generally contains a wide range of trace elements substituting on both cation and anion sites, which may exert dominant control over the geochemical behavior of trace components like Mn, Y, Sr, U, Th, and rare earth elements (REEs) in melts and magmatic fluids [8,20]; (3) the geochemical composition of apatite depends on source rock types and is unlikely to change with weathering, transport, and even burial diagenesis [20,21,27–29].

The Okinawa Trough (OT), as a typical back-arc basin in the East China Sea (Figure 1a), has been covered by thick sedimentary deposits because of continuous sedimentation by terrigenous sediments from the surrounding East Asian continent since the late Quaternary [5,30–32]. In recent decades, the clay mineral, element, and isotope compositions of the core sediments have been applied to investigate changes in sediment sources in the OT during the late Quaternary [5,7,31–39]. These techniques have improved our understanding of sedimentary processes and paleoenvironmental evolution in the OT, as well as the potential forcing mechanisms for variations in sediment sources. Substantial changes in ocean currents (especially the Kuroshio Current), sea level, fluvial runoff, and monsoon climate have been responsible for the transport and deposition regime of detrital sediment in the OT since the late last glaciation [5,32,34,40–42]. However, less attention has been paid to the source rock types of terrigenous sediment in the OT. The reconstruction of changes in sediment provenance is still primarily limited to the use of proxies from bulk elemental geochemical and clay mineralogical methods [5,38,39]. The identification of sediment provenance in the source area based on the geochemistry of heavy minerals has rarely been undertaken for the sediments in the OT. The southern Okinawa Trough (SOT) (Figure 1b) is the deepest part of the OT and is characterized by an relatively high sedimentation rate (generally > 0.1 cm/yr) [43], providing us with an ideal area and a rich archive for studying continent–ocean interactions and paleoenvironmental changes in the northwestern Pacific marginal seas during the late Quaternary [5,34]. We retrieved a high-resolution (~140 cm/kyr) sedimentary archive from the slope setting of the SOT (Core S3; Figure 1a,b), aiming to study the geochemical characteristics and sedimentological significance of individual heavy minerals in this area for the first time.

Here, we present the electron probe microanalyzer (EPMA) and laser ablation inductively coupled plasma mass spectrometry (LA-ICP-MS) geochemical data of detrital apatite in Core S3 from the SOT. The objectives of this study were to (1) characterize the geochemical compositions of detrital apatite from the SOT; (2) identify the source/ultimate source rock types of sediment in the SOT; (3) reveal the changes in provenance of sediment deposited in the SOT since 3000 cal. yr BP. The results provide new insights into sediment provenance discrimination in the study area in the past 3000 years.
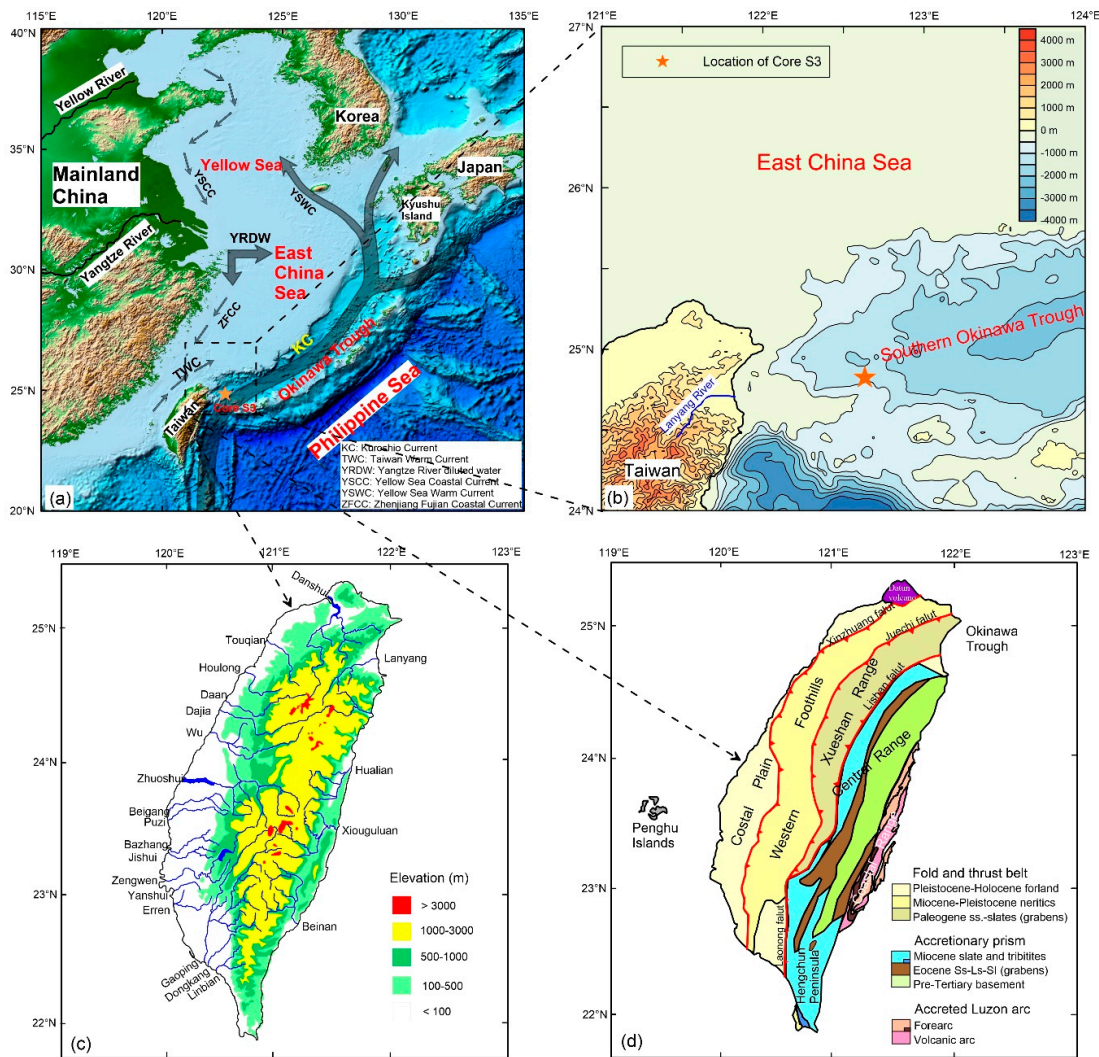
Figure 1. Map of the study area showing the location of Core S3 (**a**,**b**); ocean currents modified after Reference [38]), the major hydrographic network in Taiwan Island (**c**); modified after Reference [44]), and the tectonic map of Taiwan Island (**d**); modified after Reference [45]).

2. Regional Settings

Taiwan Island is located at the collisional boundary between the Eurasian Continental Plate and the Philippine Sea Plate [46,47]. Taiwan can be divided into three tectonic domains according to its tectonic evolution in the Cenozoic, which from east to west are a forearc basin–volcanic arc (Coastal Range), an accretionary prism (Central Range and Hengchun Peninsula), and a fold–thrust belt (Xueshan Range, Western Foothills, and Coastal Plain) (Figure 1d) [45,48]. The whole island is covered mainly by marine sedimentary rocks and metamorphic rocks. The Coastal Range consists of Oligocene–Miocene andesitic lavas and pyroclastic rocks and a set of thick Pliocene–Pleistocene forearc basin volcanic sedimentary successions. The Central Range can be divided into two parts: the western part consists of Miocene turbidite clastic rocks–slate, and the eastern part is composed of Eocene metamorphic sandstone–slate and metamorphic rocks of the Mesozoic–Paleozoic Dananao Group. The Hengchun Peninsula is mainly covered by a middle–late Miocene deep-sea turbidite layer. The Xueshan Range also contains shallow-sea facies deposits and consists of Eocene slate and sandstone and Oligocene shale. The Western Foothills are dominated by Oligocene–Pleistocene shallow-sea facies siliciclastic deposits. The Coastal Plain is a part of a foreland basin composed of late Pleistocene–Holocene fluvial deposits. Only a few igneous rocks are found in Taiwan, and are mainly distributed in Datun volcano, Jilong volcano, the Coastal Range, and the Penghu Islands. The former three are mainly composed of

andesite and quartz andesite, while the latter are mainly basalt [45,46,49,50]. Taiwan Island is situated in a tectonically active setting with a tropical to subtropical climate and frequent earthquakes and typhoons [46]. It has an extremely high physical erosion rate (3–6 mm/yr) [51] in response to its strong tectonic uplift [46]. Rivers in Taiwan Island (Figure 1c) discharge large amounts of suspended sediment into the ocean every year (180–380 Mt/yr) [51,52], and, at present, the fluvial runoff from the mountain ranges in Taiwan has become the main source of detrital sediment supply to the surrounding offshore basins [34,53].

The OT is a typical back-arc basin situated at the active plate boundary between the Eurasian Continental Plate and the Philippine Sea Plate. The SOT is adjacent to the northeast side of Taiwan (Figure 1a,b). The Lanyang River carries 6–9 Mt of sediment load directly into the southernmost OT every year, making the SOT an important "sink" of terrigenous sediment from northeastern Taiwan [54–57]. In addition, a portion of detrital sediments discharged from the rivers in western and eastern Taiwan can be delivered northward by ocean currents (i.e., Taiwan Warm Current and Kuroshio Current; Figure 1a) to the SOT [57]. Furthermore, the Yangtze River delivers 470 Mt of terrigenous sediments annually to the East China Sea, a small portion of which can be carried to the SOT over long distances by the current system in the East China Sea [34,58].

3. Materials and Methods

3.1. Sampling and Age Model

Core S3 was recovered from the slope of the SOT (24°49.42′ N, 122°37.98′ E) at a water depth of 1351 m during the HOBAB-4 cruise of the R/V Science in 2016. This 420 cm long sediment core was mainly composed of gray clayey silt. The age model for Core S3 was established based on accelerator mass spectrometry (AMS) ^{14}C dating of mixed planktonic foraminifera picked from eight horizons [59]. The depositional age at the lower boundary was estimated as 3 ky BP. Continuous 10 cm sections (more than 200 g) were picked from Core S3, and each served as one Section for single mineral selection to ensure sufficient samples for geochemical analysis. In this study, four sections were chosen for selection of detrital apatite; the sedimentary age of each Section was constructed using the BACON software package (version 2.3.9.1) [60].

3.2. Analytical Methods

The detrital apatites analyzed in this study were separated from the chosen four sections using conventional heavy liquid and magnetic techniques. More than 150 apatites picked from each Section under a binocular microscope were mounted in epoxy and then polished by diamond abrasive for determination of major and trace element compositions. All of the analyses were performed on the central part of each apatite. The analyzed apatite numbers for major and trace element compositions are listed in Table 1.

Table 1. The corresponding layers and sedimentary ages [59] and the analyzed apatite number of the four sections in Core S3.

Sections	Depth (cm)	Sedimentary Ages (cal. yr BP)	Number of Analyses (EPMA)	Number of Analyses (LA-ICP-MS)
Section 1	404–414 cm	2775–2920	44	16
Section 2	326–336 cm	1875–1950	59	35
Section 3	249–259 cm	1340–1400	46	23
Section 4	89–98 cm	385–435	32	20

EPMA: electron probe microanalyzer; LA-ICP-MS: laser ablation inductively coupled plasma mass spectrometry; cal. yr BP: calibrated years before present.

Major element compositions of the apatite were analyzed with a JXA-8230 EPMA at the State Key Laboratory of Continental Dynamics in Northwest University, Xian, China. The analysis was

carried out under conditions of 15 kV accelerating voltage, 20 nA beam current, and a 10 μm diameter beam. Natural/synthetic mineral standards were from the SPI Company, USA. The standards used for element content calibrations were apatite for Ca, P, and F; NaCl for Cl; celestite for Sr; rhodonite for Mn; anhydrite for S; olivine for Mg; albite for Na; and magnetite for Fe.

Trace element compositions of the apatite were conducted by LA-ICP-MS at the Wuhan SampleSolution Analytical Technology Co., Ltd., Wuhan, China. Detailed operating conditions for the laser ablation system and the ICP-MS instrument and data reduction were similar to those described in Reference [61]. a GeolasPro laser ablation system consisting of a COMPexPro 102 ArF excimer laser (wavelength of 193 nm and maximum energy of 200 mJ) and a MicroLas optical system were used for laser sampling, and ion-signal intensities were acquired using an Agilent 7900 ICP-MS instrument. Helium was applied as a carrier gas. Argon was used as the make-up gas and mixed with the carrier gas via a T-connector before entering the ICP. a "wire" signal smoothing device was included in this laser ablation system [62]. The spot size, repetition rate, and energy of the laser were set to 32 μm, 5 Hz, and 80 mJ, respectively. The trace element compositions of apatite were calibrated against various reference materials (BHVO-2G, BCR-2G, and BIR-1G), and the Ca content obtained by EPMA was used as the internal standard [63]. NIST SRM 610 was measured periodically to monitor the overall analytical stability. Each analysis included a 20–30 s background measurement (laser-off) followed by 50 s data acquisition from the sample. After the analytical procedures, off-line selection and integration of background and analyzed signals, time-drift correction and quantitative calibration for trace element analysis were performed using the Excel-based software ICPMSDataCal 10.8 [63].

The separated heavy minerals were also subjected to qualitative and semi-quantitative analysis using stereomicroscopy and polarizing microscopy.

4. Results

Four sections from the bottom to top of Core S3 were chosen for apatite separation. From Section 1 to Section 4, the corresponding layers and sedimentary ages of each Section are shown in Table 1. Representative transmitted-light photomicrographs of apatites from the four sections of Core S3 are shown in Figure 2. The majority of apatite grains from the SOT were irregular or round and somewhat broken, while some of them were columnar, euhedral, and relatively intact.
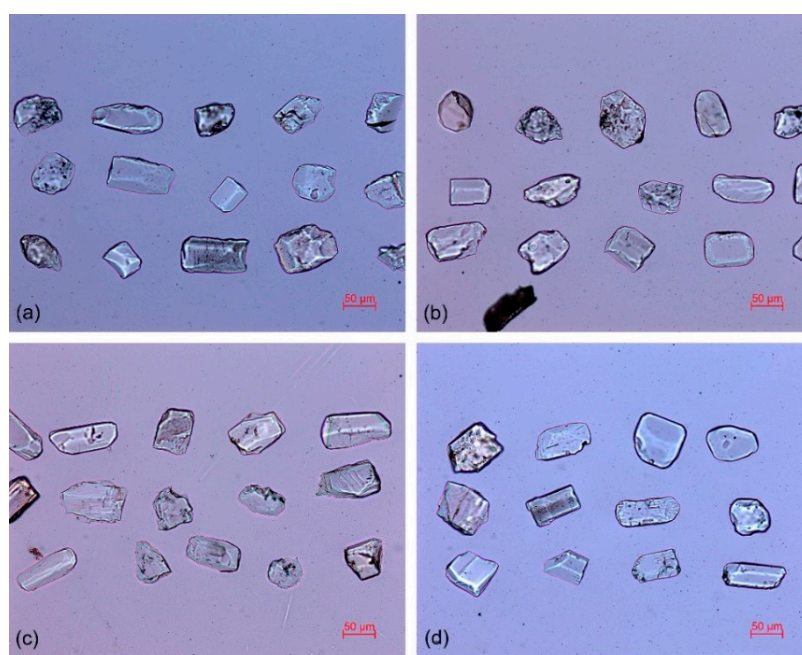
Figure 2. Transmitted-light photomicrographs showing examples of detrital apatites from the four sections of Core S3. Section 1 (**a**), Section 2 (**b**), Section 3 (**c**), and Section 4 (**d**).

The major element compositions of detrital apatites in the four sections of Core S3 from the SOT are listed in Supplementary Table S1. The major element composition showed that the detrital apatites in this study were relatively pure and mainly consisted of Ca, P, O, and F, with almost no Mg or Na (Supplementary Table S1), which is different from bioapatite which has relatively high contents of Na and Mg [64]. The Ca concentrations and F concentrations in almost all of the apatites were more than 39 wt.% and lower than 3 wt.%, respectively (Supplementary Table S1), indicating that authigenic overgrowths of detrital apatite did not occur in this study, which generally have Ca concentrations lower than 38 wt.% and F concentrations higher than 4 wt.% [25]. The trace element (Mn, Sr, Y, Th, and U) and rare earth element (REE) compositions of detrital apatites in the four sections of Core S3 from the SOT are listed in Supplementary Table S2. The calculated parameters and ratios such as La/Nd, (La + Ce + Pr)/ΣREE(%), Eu/*Eu, and (Ce/Yb)$_{cn}$, based on the trace element and REE compositions of detrital apatite that were used in the following text, are detailed in Supplementary Table S3. The relative abundances of apatites fell into the four fields of the La/Nd vs. (La + Ce + Pr)/ΣREE(%) plot are listed in Table 2. The proportions of apatites with Th/U>1 and Th/U<1 in the four sections of Core S3 are also shown in Table 2. The heavy mineral compositions of the bulk sediment in the four Section and the calculated heavy mineral indices are listed in Supplementary Table S4.

Table 2. Classification of apatites according to La/Nd vs. (La + Ce + Pr)/ΣREE(%) diagram and Th/U ratios.

| Sections	Acidic (%)	Mafic/Intermediate (%)	Alkaline–Mafic/Intermediate (%)	Alkaline (%)	Th > U (%)	Th < U (%)
Section 1	43.8	31.3	6.3	18.8	93.8	6.3
Section 2	54.3	31.4	5.7	8.6	57.1	42.9
Section 3	47.8	34.8	4.3	13.0	43.5	56.5
Section 4	55.0	15.0	15.0	15.0	60.0	40.0

5. Discussion

5.1. Provenance Discrimination Diagrams

Apatite is a common accessory mineral in the three major rock categories (i.e., igneous, metamorphic, and sedimentary rocks), and the variations in trace elements such as Mn, Sr, Y, Th, U, and REEs in apatite mainly depend on the types of host rock [20,27]. For example, in igneous rocks, the trace element composition in apatite is closely related to the whole-rock SiO$_2$ content; Mn, Y, and heavy REEs (HREEs) are likely to become relatively enriched during magmatic differentiation, but Sr becomes relatively depleted [21]. Therefore, the trace element compositions and element ratios of apatite can be used as important indicators to distinguish the host rock types. Provenance discrimination studies based on apatite geochemistry have demonstrated many methods for the classification of detrital apatite grains [20,65,66], which have been successfully adopted and improved in recent research [8,21–23]. In this study, various strategies from the literature were combined to understand the geochemical information recorded in the detrital apatites from the SOT.

5.1.1. REE Distribution Patterns in Apatite

The REE composition in apatite is mainly dependent on the geochemical composition and fractionation degree of the host rock; thus, apatite grains from host rocks with different compositions and magmatic differentiation degrees appear to have differently shaped chondrite-normalized REE patterns [20,21]. Apatites from mafic rocks and alkaline rocks tend to have light REE (LREE)-enriched profiles [20,67], whereas apatites from S-type and felsic I-type granites and most metamorphic rocks are characterized by flat (slightly upward–convex) to LREE-depleted patterns [28,65,68]. The geochemical behavior of REEs in apatite is considered to reflect its competition for these elements with other REE-carrier minerals [8,29]. For example, the preferential crystallization of LREE-enriched minerals such as monazite, allanite, epidote, and feldspar usually leads to significant LREE depletion in apatite

grown from highly fractionated granites and in apatite crystallized in metamorphic rocks [29,69,70]. The crystallization of HREE-enriched minerals such as xenotime, garnet, and zircon prior to the growth of apatite may result in HREE-depleted profiles in apatite [8,29,71,72]. The display of negative Eu anomalies in apatite REE patterns occurs mainly because the crystallization of feldspar removes much Eu^{2+} from the melt [20,21,72]. Apatite from less fractionated mafic rocks is characterized by a lack of positive or negative Eu anomalies, while the presence of significant negative Eu anomalies is a common feature of apatite from highly evolved granites and granite pegmatites [28,29]. The chondrite-normalized REE patterns were plotted for detrital apatites from the four sections of Core S3 (Figure 3) using the chondrite values from [73]. According to visual inspection, the analyzed apatites with similar REE patterns were defined as one population in order to better understand their sources. More than four apatite populations were defined in these sections, based on the variations in their REE patterns (Figure 3).
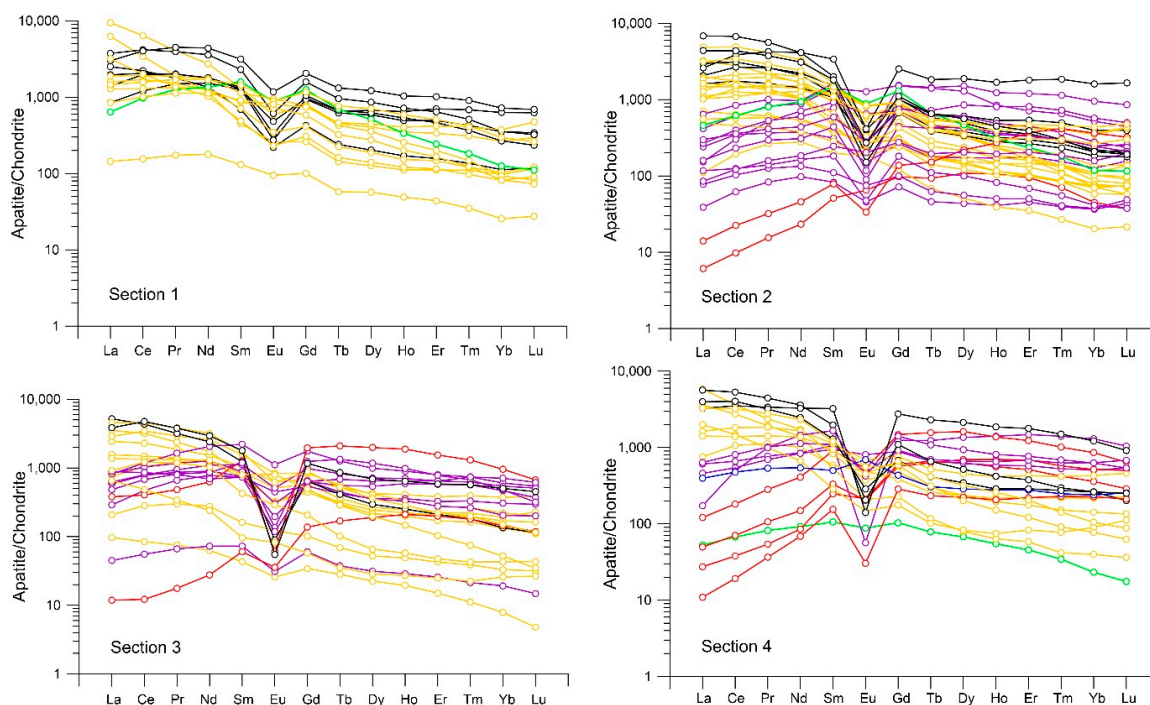

Figure 3. The chondrite-normalized rare earth element (REE) patterns of detrital apatites in the four sections of Core S3 from the South Okinawa Trench (SOT). The chondrite REE values are from Reference [73]. Note: REE patterns with deep yellow color, black color, purple, and red color indicate Population 1, Population 2, Population 3, and Population 4, respectively.

Population 1 (Figure 3, deep yellow) was characterized by moderately enriched LREEs with no or only slightly negative or positive Eu anomalies. The REE patterns in this population were similar to those of apatite from relatively unfractionated, more mafic sources (e.g., syenite, lherzolite, and carbonatites) [20–22,74]. Population 2 (Figure 3, black) also yielded moderately enriched LREE profiles but showed significant negative Eu anomalies. This pattern is normally present in apatite from magmatic iron deposits [75], diabase [20], mafic I-type granites [28], and dacite [76]. Population 3 (Figure 3, purple) showed relatively flat REE profiles, and the majority of grains had moderate to strong negative Eu anomalies, with slight depletions in LREEs and HREEs relative to middle REEs (MREEs). Flat REE patterns with significant negative Eu anomalies are a common feature of apatites from S-type granites, felsic I-type granites, and granitic pegmatites [20,28,29]. However, flat REE patterns with slight negative Eu anomalies can be found in apatite from migmatites [77]. This type of REE pattern can also be observed in apatite from metamorphic rocks because of geochemical reequilibration under metamorphic conditions [8,77]. Population 4 (Figure 3, red) displayed moderately to strongly

depleted LREEs with significant negative Eu anomalies (with the exception of one grain in Section 3, which lacked an Eu anomaly). In general, apatite with this type of REE pattern is closely related to strongly fractionated granitic source rocks or metamorphic rocks [23,29,70]. Their extremely low Sr concentrations (generally <250 µg/g) correspond well to a felsic source [23]. The grain with a high Sr concentration (1178 µg/g) and no Eu anomaly may have had a metamorphic origin (e.g., mafic blueschist) [78]. The remaining grains (Figure 3, green) were strongly depleted in HREEs, with the relatively convex–upward REE patterns observed in eclogites [79]. The analyzed apatites from Section 2, Section 3, and Section 4 showed greater diversities of REE patterns (having more apatite populations) than those from Section 1 (Figure 3), suggesting that the apatites in Section 1 may have derived from a source with fewer rock types.

5.1.2. La/Nd vs. (La + Ce +Pr)/ΣREE Discrimination Diagram

Reference [65] found that the LREEs in apatite from different types of host rock showed evident gradient changes, and proposed the La/Nd vs. (La + Ce +Pr)/ΣREE diagram as a useful tool to categorize apatites from acidic, intermediate-mafic, or alkaline rocks. The apatites in Section 1, Section 2, Section 3, and Section 4 analyzed from Core S3 were plotted on a La/Nd vs. (La + Ce + Pr)/ΣREE diagram (Figure 4). All of the grains from the four sections had wide ranges of La/Nd and (La + Ce + Pr)/ΣREE ratios (plotting extensively in the acidic, mafic/intermediate, and alkaline fields). Apatite in Section 1 tended to have higher (La + Ce +Pr)/ΣREE ratios and lower proportions plotted in the acidic field than in other sections (Table 2), suggesting that the source of apatite in Section 1 included a lower proportion of evolved rocks than were found in the other sections.
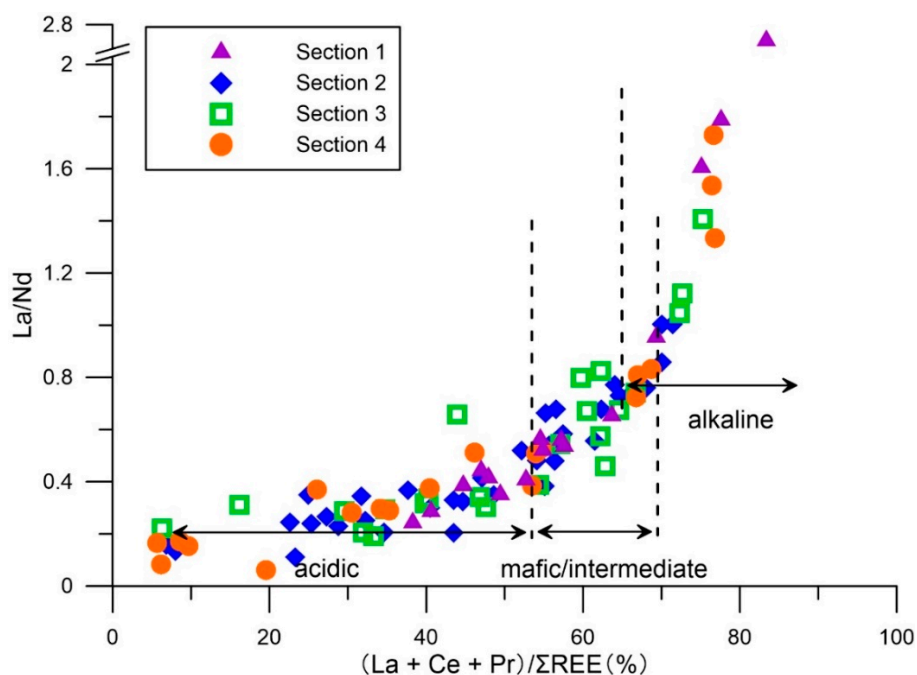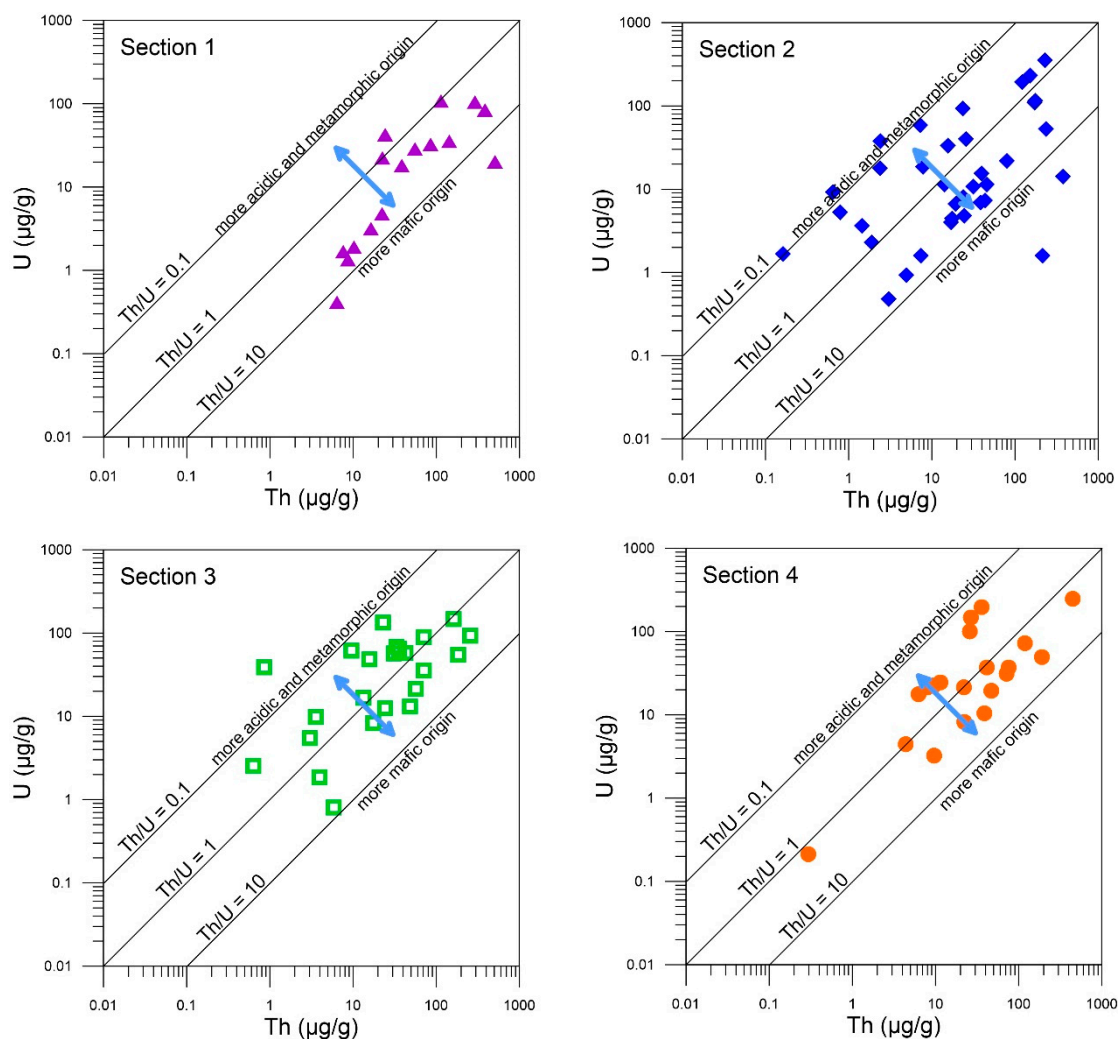

Figure 4. Detrital apatite compositions in the four sections of Core S3 from the SOT plotted on the La/Nd vs. (La + Ce + Pr)/ΣREE (%) classification plot [65].

5.1.3. Th vs. U Binary Plot

The Th vs. U binary plot that was first proposed by Reference [66] has also been successfully applied to discriminating the provenance of detrital apatite [8,21–23]. The depletion in Th relative to U (Th < U) in apatite is generally caused by the growth of monazite and epidote, which preferentially concentrate Th before the crystallization of apatite. This phenomenon usually occurs during the diagenetic processes of highly evolved rocks or metamorphic rocks (especially from metapelites),

suggesting that detrital apatites with Th < U may have a highly fractionated source or a metamorphic origin [20,26,28,70]. Reference [70] suggested that metamorphic apatites from low- to medium-grade metapelites and metabasites usually concentrate extremely low Th, REEs, and Y, which can further distinguish these detrital apatites from granitic apatite. The Th and U concentrations of the analyzed apatites from Core S3 are plotted in Figure 5. Most of the apatites (>93.8%) from Section 1 tended to have Th higher than U (6–508.9 µg/g Th, 0.4–107.7 µg/g U) and plot on the Th-enriched side of the Th/U = 1 or even Th/U = 10 lines, suggesting that most of the detrital apatites deposited in Section 1 had a relatively unfractionated, more mafic source [21,22,66]. Samples from the younger sections (i.e., Section 2, Section 3, and Section 4) tended to have more dispersed Th and U concentrations and plot on both sides of the Th/U = 1 line (Figure 5). According to recent studies [8,21,28], apatites with low Th/U ratios (<1) indicate that some of detrital apatites in these sections originated from granitoids, granite pegmatites, migmatites, and metasediments. Several apatite grains with extremely low Th and U concentrations were observed in these sections (Figure 5), suggesting that apatites from metapelites or metabasites may have partly contributed to these sections [70]. Therefore, the Th vs. U plot suggests that detrital apatites in Section 2, Section 3, and Section 4 were derived from a mixture of mafic, acidic, and metamorphic lithologies.
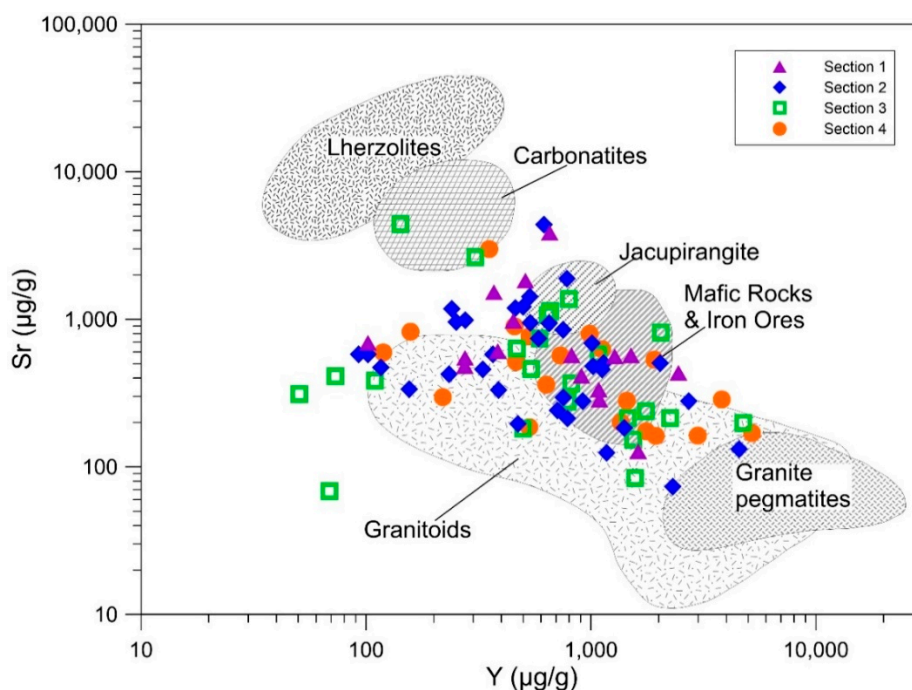

Figure 5. Detrital apatite compositions in the four sections of Core S3 from the SOT plotted on a Th vs. U binary plot [66].

5.1.4. Plots of Sr vs. Y and Mn, (Ce/Yb)$_{cn}$ vs. ΣREE, and Y vs. Eu/Eu*

Reference [20] studied the geochemical behavior of trace elements and REEs in apatite from a series of intrusive rocks, and proposed that Sr vs. Y, Mn, (Ce/Yb)cn vs. ΣREE, and Y vs. Eu/Eu* plots can be used for provenance studies; these discrimination diagrams have been well applied in recent studies [8,21,22]. Therefore, these plots were further used for systematic comparative studies to discriminate the sources of detrital apatites from Core S3.

The apatites in Section 1 tended to have less scattered Sr and Y concentrations than those from other sections, and most of the grains fell within and near the fields of mafic rocks and iron ores and jacupirangite (Figure 6). The apatites from Section 2, Section 3, and Section 4 were characterized by more variable Sr and Y concentrations (some of them had higher Sr and lower Y contents). Many of the apatites in these sections were also located in the fields of mafic rocks and iron ores and jacupirangite, and others plotted in the field of granitoids (Figure 6). In general, Sr concentration decreases and Y concentration increases in apatite with the degree of magmatic fractionation [20]. For example, apatites from ultramafic and carbonatitic rocks tend to have extremely high Sr concentrations and low Y concentrations [20]. In comparison, the Sr vs. Y plot implied that detrital apatites deposited in different sections of Core S3 all had an unfractionated and mafic source, and that a larger proportion of apatites from Section 2, Section 3, and Section 4 may also have had an evolved source.
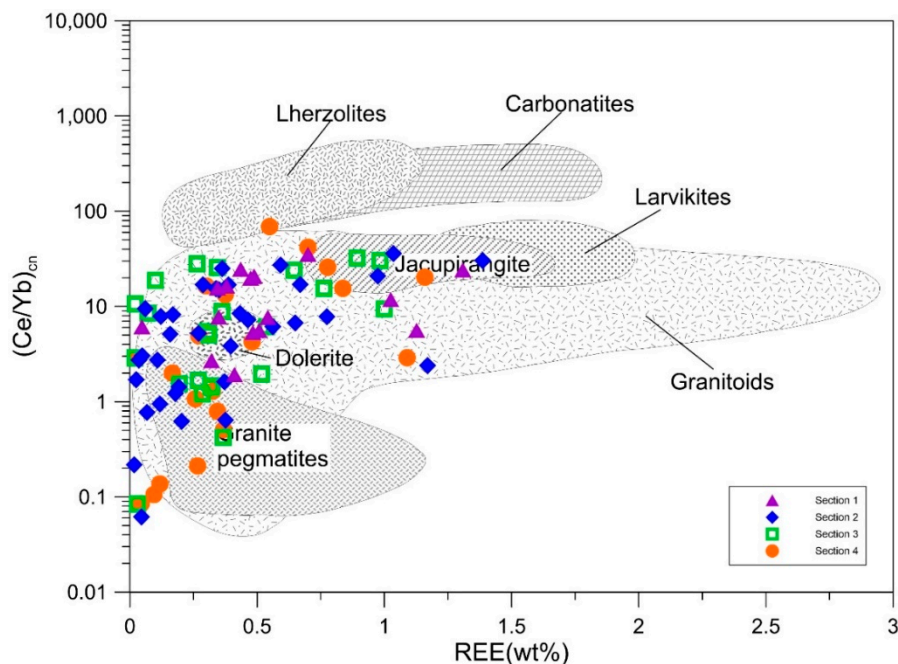

Figure 6. Sr vs. Y genetic plot proposed by Reference [20] showing the analyzed apatite compositions in the four sections of Core S3 from the SOT.

The Sr vs. Mn plot is capable of distinguishing between apatites from mafic rocks or iron ores and those from granitoids [20], and usually mirrors the Sr vs. Y plot [21]. Detrital apatites from Section 2, Section 3, and Section 4 tended to have more scattered Sr and Mn concentrations than those from Section 1 (Figure S1). a portion of grains from Section 2, Section 3, and Section 4 with low Sr contents and disordered Sr contents plotted in the field of granitoids and granite pegmatites, indicating that these sections contained a greater percentage of detrital apatites originating from highly evolved rocks.

The steepness of the REE pattern (the degree of LREE enrichment) can be well defined by the (Ce/Yb)$_{cn}$ value. The (Ce/Yb)$_{cn}$ values of apatites generally decrease from ultramafic rocks (including carbonatites) through mafic/intermediate rocks to highly evolved acidic rocks [20]; thus, the (Ce/Yb)$_{cn}$ vs. ΣREE plot can also be used to distinguish apatites from various rocks [20–22]. The majority of

apatites in Section 1 (up to 88%) were characterized by relatively strong LREE enrichments with $(Ce/Yb)_{cn} > 3$. In addition, many grains had relatively strong LREE enrichments $(Ce/Yb)_{cn} > 3)$ in Section 2, Section 3, and Section 4, with values of 66%, 61%, and 45%, respectively. These grains plotted in or near the fields of dolerite, jacupirangite, and lherzolite (Figure 7), suggesting that detrital apatites deposited in these sections all had a source with relatively unfractionated mafic rocks. a quantity of grains in Section 2, Section 3, and Section 4 tended to have slightly enriched to significantly depleted LREE profiles with $(Ce/Yb)_{cn} < 3$, and many of them plotted in the field of granite pegmatites, which was absent in Section 1 (Figure 7). This result implies that larger proportions of detrital apatites deposited in Section 2, Section 3, and Section 4 are from highly evolved sources.

Figure 7. $(Ce/Yb)_{cn}$ vs. ΣREE genetic plot proposed by Reference [20], showing the analyzed apatite compositions in the four sections of Core S3 from the SOT.

The Y vs. Eu/Eu* plot showed that the majority of apatites in Section 1 and high proportions of apatites in Section 2, Section 3, and Section 4 were characterized by relatively small Eu anomalies with Y concentrations between 100 and 1000 μg/g (Figure S2). In addition, small portions of the apatites in Section 2, Section 3, and Section 4 tended to have significant negative Eu anomalies with relatively high Y contents (>1000 μg/g) (Figure S2). Both the amplitude of the negative Eu anomaly and the Y content usually become greater with increasing fractionation [20]. This result suggests that detrital apatites deposited in the four sections all had a source from mafic/intermediate rocks, while Section 2, Section 3, and Section 4 included higher proportions of detrital apatites derived from strongly fractionated acidic rocks such as granites and pegmatites.

Several apatite grains plotted outside the genetic fields corresponding to different types of igneous rocks (Figures 6 and 7, Supplementary Figures S1 and S2), and we inferred that these apatites may have had a metamorphic origin [8]. Unfortunately, in the present study we could not make comprehensive comparisons due to the lack of a systematic database with the chemical compositions of metamorphic apatites.

5.1.5. Principal Component Analysis Plot

The principal component analysis (PCA) plot can also be used to discriminate the provenance of detrital apatite [80]. The analyzed apatites from the four sections were plotted with apatites from various rocks with diverse compositions from the literature on a PCA plot (Figure 8), using the "Vegan:

Community Ecology" package for R language [81]. The majority of detrital apatites in Section 1 were compositionally similar to apatites from mafic/intermediate rocks [76,82], plotting intermediately among basic, intermediate, and metamorphic rock end-member compositions. The detrital apatites in Section 2, Section 3, and Section 4 tended to have more scattered trace element and REE compositions, widely plotting within/near the end-member compositions of mafic/intermediate, acidic, and metamorphic rocks [28,70,76,82]. These results also suggested that apatites in Section 1 were derived from fewer rock types than other sections, which is in agreement with the results obtained from other plots (e.g., Figures 5–7).
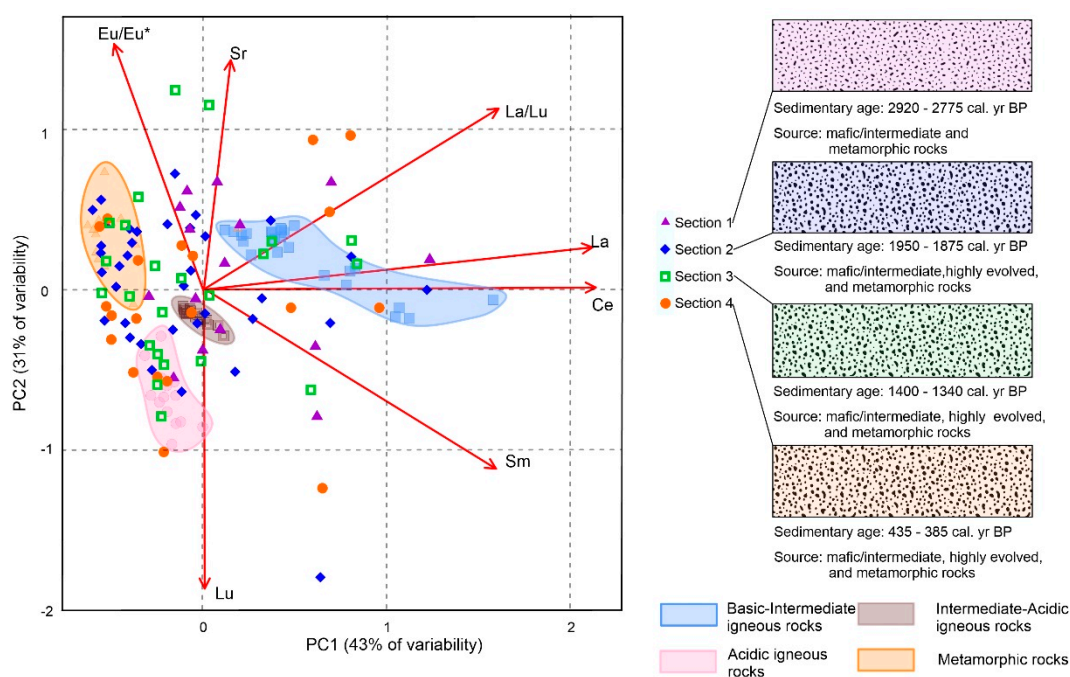

Figure 8. Biplot of the principal component analysis [81] results of apatite compositions in the four sections of Core S3 from the SOT compared to apatite data in different types of bedrock from the literature [28,70,76,82]. The principal component 1 (PC1) vs. PC2 plot explained >74% of the variability in the data. The vectors (red arrows) point in the direction most similar to the variability in element contents and ratios [23,80]. Apatites in more mafic rocks are generally enriched with LREEs and depleted in HREEs [20,67,82], and are hence "pulled" toward the La/Lu, La, and Ce vectors [80]. Apatites in acidic rocks (e.g., S-type granite) are characterized by flat REE patterns, extremely negative Eu anomalies, and low Sr contents [28], which "push" apatite data away from the La/Lu, Sr, and Eu/Eu* vectors and toward the Lu (HREE) vectors [80]. Apatites in metamorphic rocks (e.g., metapelite and metabasite) are characterized by high Sr contents, flat or positive Eu anomalies, and low REE contents [70]; thus, metamorphic apatites are "pulled" toward the Sr and Eu/Eu* vectors and "repelled" by the REE vectors [80]. Apatites in intermediate–acidic rocks (e.g., dacite) are usually scattered near the beginning point of the vectors.

5.2. Implications for Sediment Provenance

5.2.1. Controls on Detrital Apatites in the Four Sections

The effects of other factors on sedimentary mineralogy and geochemistry should be well evaluated to ensure that our apatite assemblage can adequately reflect the characteristics of source rock types. The mineralogical and geochemical compositions of sediment discharged from rivers to the ocean reflect the combination of a series of processes [3,4]. Ocean currents (especially the Kuroshio Current), sea level, and monsoon climate are considered the main factors responsible for the transport and depositional regime of detrital sediments in the SOT [5,34]. Hydraulic sorting of mineral grains caused

by changes in ocean currents generates mineral assemblages and geochemical trends that are not driven by variations in erosion and weathering of the source region [3]. During transgressive periods, variations in sea level can lead to erosion and reworking of older deposits at the shoreline which are then mixed with newly discharged sediment, which also alters the mineralogical and geochemical composition of sediments [3]. Although the intrusion time and intensity of the Kuroshio Current in the SOT since the late Quaternary has been controversial in recent decades [5,34,40,42,83,84], the pathway and intensity of the Kuroshio Current have been relatively stable during the late Holocene (Figure 1). In addition, the modern oceanic circulation patterns in the study area fully developed before the late Holocene (Figure 1) [7,42]. No significant change in sea level has occurred since the late Holocene (Figure 9a) [85]. The effect of diagenesis (authigenic minerals) on the sedimentary mineralogy and geochemistry of Core S3 can be neglected because the core was shallowly buried (420 cm long) with a high sedimentation rate (140 cm/kyr). No reversed ^{14}C age was observed, indicating that the effect of reworking sediments was also insignificant [4], consistent with ocean currents and the sea level remaining stable during the late Holocene. These findings suggest that ocean currents, sea level, and diagenesis were not the main controlling factors of apatite assemblage differences between Section 1 and other sections. The climate in the study area is dominated by the East Asian monsoon system [5,34], while monsoon precipitation and temperature indicated by δ^{18}O records of the Dongge Cave stalagmite remained relatively stable between 3000 and 500 cal. yr BP and slightly increased after 500 cal. yr BP (Figure 9b) [86]. This suggests no direct relationship between monsoon climate and detrital apatite assemblage in the four sections. Therefore, the apatite assemblages in this study can be used to reconstruct changes in provenance of Core S3 since 3000 cal. yr BP.
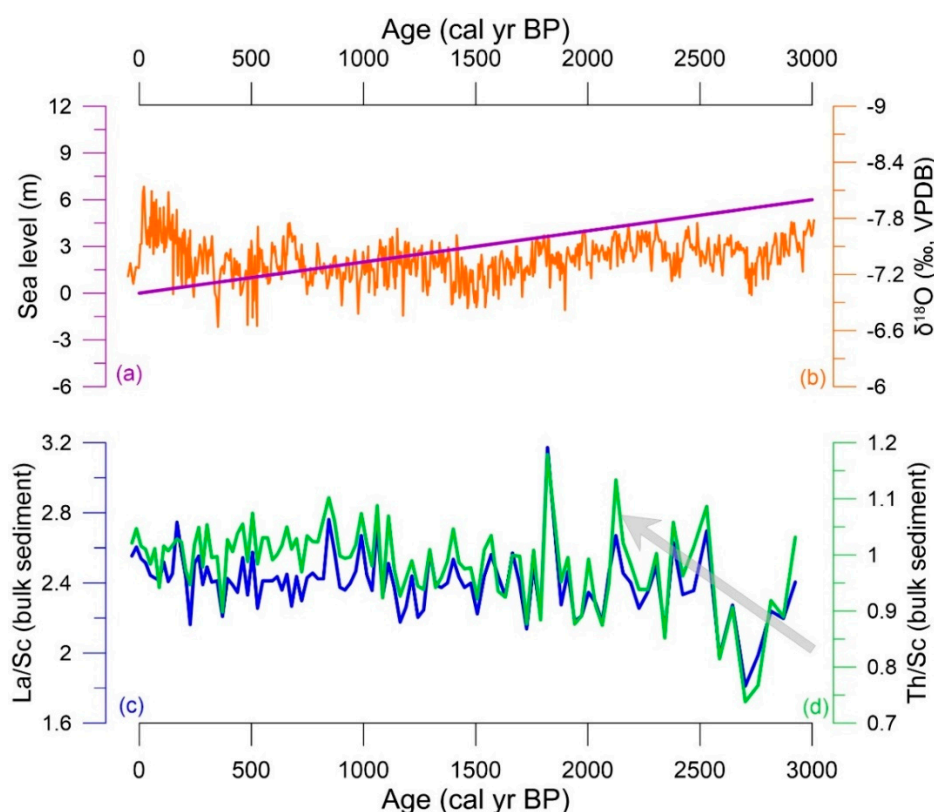
Figure 9. Temporal variations in sea level change [85] (**a**), δ^{18}O records of the Dongge Cave stalagmite [86] (**b**), and La/Sc (**c**) and Th/Sc (**d**) of the bulk sediments in Core S3 since 3000 cal. yr BP.

5.2.2. Changes in Provenance

Much valuable provenance information about the source rocks was detected in the sediments of Core S3 based on the geochemical compositions of the detrital apatites. a series of discrimination plots (Figures 4–8) demonstrated clearly that the detrital apatites deposited in Core S3 since 3000 yr BP were derived from a mixture of sources, including ultramafic–mafic rocks, intermediate and alkaline rocks, and highly evolved rocks such as granites and granitic pegmatites, as well as from metamorphic rocks. The analyzed apatites in the earliest sedimentary Section (i.e., Section 1) of Core S3 from the SOT tended to have fewer rock types and a lower proportion of highly evolved rocks compared with those in other, younger sections (Figures 4–7), indicating changing provenance. This change is clearly shown in Figure 8. The REE and trace element compositions of apatites in Section 1 were different from those in other sections, while the younger three sections showed strong geochemical similarities. La and Th are usually enriched in siliceous rocks, while Sc is usually enriched in basic rocks [87]. Therefore, low La/Sc and Th/Sc ratios can be interpreted to indicate less sediment flux from acid igneous sources [48]. The bulk sediment in Section 1 had lower La/Sc and Th/Sc ratios than the younger sections (Figure 9c,d), suggesting that sediment in Section 1 had lower erosional flux from acid igneous rocks and that sediment sources changed in other sections, which also agreed well with our geochemical evidence from detrital apatites. Comparing our results with results from recent studies, the apatite assemblages in Core S3 were similar to those found in sandstones [8,21–23], indicating that the late Holocene sediment in the SOT was derived from a source area with extremely heterogeneous lithologies or from a source area mainly composed of sedimentary rocks that had an ultimate source containing a wide range of rock types.

Core S3 was located at the continental slope of the southernmost OT, closely adjacent to the northeastern tip of Taiwan Island (Figure 1). During the late Holocene, the source of detrital sediment in the SOT was dominated by terrigenous supply from Taiwan rivers, while the contribution of sediment from mainland China was relatively small, which has been well demonstrated in many studies, including in sediment traps [57], clay mineral composition [34], and isotope composition of core sediments [5,59]. In addition, the Lanyang River in northeastern Taiwan is the only river that has been able directly supply terrigenous sediment to the SOT (6–9 Mt/yr) during the late Holocene [54,55,57]. The total proportion of unstable heavy minerals (e.g., pyrite, augite, epidote, amphibole) in Core S3 was much higher than that of stable heavy minerals (e.g., zircon, rutile, tourmaline, garnet, anatase, leucoxene, apatite, magnetite, ilmenite) (Supplementary Table S4). Many grains in both stable and unstable minerals have sharp edges and corners, and a relatively high content of rock fragments can be observed in the heavy mineral fraction. The ZTR index (zircon % + tourmaline % + rutile %) has been widely used to reflect the transport distance and source direction of the sediments [88]. The ZTR values in the four sections were lower than 5.1 (Supplementary Table S4). These results strongly suggest that the heavy minerals in Core S3 have experienced weak weathering and light abrasion, and that the sediment deposited in Core S3 was close to the provenance area with short distance transportation (i.e., Taiwan Island). Taiwan Island is characterized by widely distributed Cenozoic strata and is mainly composed of marine sedimentary outcrops, such as sandstone, siltstone, and shale, with scattered limestone outcrops [47]. Sedimentary rocks and slightly metamorphosed sedimentary rocks account for 86% of the total area of Taiwan Island, and the remaining 14% is mainly covered by metamorphic rocks [89]. The outcrops of igneous rocks on Taiwan Island are relatively few and are mainly on the Penghu Islands, in the Datun and Jilong volcanic groups in northern Taiwan, and in the Coastal Range of eastern Taiwan. The first area mainly consists of basalt, and the remaining three areas consist of andesite and andesitic clastic rocks [46,89]. There are clearly not enough igneous rocks in the river drainage basins of Taiwan Island to be the source of the detrital apatites deposited in Core S3. Because sedimentary rocks and metamorphic rocks are widely distributed in the river drainage basins of Taiwan Island and contain the apatite assemblages from all the rock types noted in the discrimination plots, the weathering and erosion products of sedimentary and metasedimentary rocks could be the main sources from which most clastic sediments in the SOT are derived. The analyzed apatites in each

Section were heterogenous in composition; all of the grains were randomly distributed within/near the rock end-member compositions on the PCA plot (Figure 8). This is a typical feature of apatite from detrital/sedimentary provenance [80]. Reference [89] suggested that the abundant illite and chlorite in Taiwan rivers are products formed after the strong physical weathering of sandstone, shale, and slate, and Reference [47] proposed that the geochemical compositions and REE patterns of Taiwan fluvial sediment are closely associated with the sedimentary and metasedimentary rocks in Taiwan Island. These findings further support the hypothesis that terrigenous sediments in the SOT are mainly derived from sedimentary rocks.

The river drainage basins in eastern Taiwan consist of mostly metamorphic rocks (e.g., schists, marbles, amphibolites, metadiabases, and gneisses), while the river drainage basins in western and northeastern Taiwan consist of sedimentary rocks (sandstones, siltstones, and mudstones) and meta-sedimentary rocks (e.g., slates, shales, and phyllites), implying that sediments/detrital apatites from eastern Taiwan have not significantly contributed to the SOT, which is in agreement with the isotopic evidence from Core S3 that the sediments in the SOT have isotopic compositions similar to those of river sediments in western and northeastern Taiwan, but different from those of sediments in eastern Taiwan rivers [59]. Although we were unable to obtain samples of sedimentary rocks from Taiwan for comprehensive comparison, we are confident that terrigenous sediments in the SOT are the weathered/eroded products of sedimentary rocks and meta-sedimentary rocks from the drainage basins of western and northeastern Taiwan rivers.

Because detrital apatites in Core S3 are the weathering and erosion products of basement rocks in Taiwan rivers that drain sedimentary rocks and meta-sedimentary rocks, there were negligible effects of oceanic currents, sea level, diagenesis, monsoon climate, and reworking of sediments on the detrital apatite assemblages in the four sections. We inferred that the weathered/eroded sedimentary rocks that correspond to Section 1 might derive from fewer rock types, and the ultimate sources of sediment in the younger sections tended to have more erosional flux from acid rocks than those in Section 1 (Figures 8 and 9). This could likely be responsible for the variation in apatite assemblages between Section 1 and the other sections (i.e., changes in provenance). The weathered/eroded basement rock types in the weathering profile of the Taiwan river drainage basins changed in Section 2 (2010–1940 cal. yr BP) and have remained stable since then.

6. Conclusions

Detrital apatites in four sections of a high-resolution (~140 cm/kyr) sedimentary archive from the SOT were selected for single-grain mineral chemical analysis. The analytical results suggest that apatites in all sections were derived from a mixture of sources; most apatites in Section 1 were derived from mafic/intermediate rocks, and some from alkaline rocks and metamorphic rocks. In addition to the rock types in Section 1, Sections 2, 3, and 4 also contained large proportions of apatite from highly evolved rocks. The stratigraphic evidence in the study area indicated that sediments in the SOT are the weathering/erosion products of sedimentary and metasedimentary rocks from the watersheds of western and northeastern Taiwan Island, with ultimate sources from a range of rock types. Fluvial sediment from eastern Taiwan did not significantly contribute to the deposition in the SOT. The geochemical similarity among the apatites in the younger three sections and their difference from those in Section 1 suggested that the weathered/eroded rock types in the drainage basins of Taiwan rivers changed in Section 2 (2010–1940 cal. yr BP), and have remained stable since then.

Detrital apatite is a promising accessory mineral in sediment provenance analysis and has potential value in reflecting paleoenvironmental evolution in the source area. However, the discrimination plots at present still contain many deficiencies, especially the lack of a database of apatite compositions with metamorphic origins for comprehensive comparison. Therefore, further work is required to promote our understanding of the geochemical behavior of trace elements in apatites from a larger range of lithologies.

References

1. Selvaraj, K.; Chen, C.T.A. Moderate chemical weathering of subtropical Taiwan: Constraints from solid-phase geochemistry of sediments and sedimentary rocks. *J. Geol.* **2006**, *114*, 101–116. [CrossRef]

2. Selvaraj, K.; Chen, C.-T.A.; Lou, J.-Y.; Kotlia, B.S. Holocene weak summer East Asian monsoon intervals in Taiwan and plausible mechanisms. *Quat. Int.* **2011**, *229*, 57–66. [CrossRef]

3. Hu, D.; Clift, P.D.; Boening, P.; Hannigan, R.; Hillier, S.; Blusztajn, J.; Wan, S.; Fuller, D.Q. Holocene evolution in weathering and erosion patterns in the Pearl River delta. *Geochem. Geophys. Geosyst.* **2013**, *14*, 2349–2368. [CrossRef]

4. Wan, S.; Toucanne, S.; Clift, P.D.; Zhao, D.; Bayon, G.; Yu, Z.; Cai, G.; Yin, X.; Revillon, S.; Wang, D.; et al. Human impact overwhelms long-term climate control of weathering and erosion in southwest China. *Geology* **2015**, *43*, 439–442. [CrossRef]

5. Dou, Y.; Yang, S.; Shi, X.; Clift, P.D.; Liu, S.; Liu, J.; Li, C.; Bi, L.; Zhao, Y. Provenance weathering and erosion records in southern Okinawa Trough sediments since 28 ka: Geochemical and Sr-Nd-Pb isotopic evidences. *Chem. Geol.* **2016**, *425*, 93–109. [CrossRef]

6. Huang, C.; Zeng, T.; Ye, F.; Xie, L.; Wang, Z.; Wei, G.; Lo, L.; Deng, W.; Rao, Z. Natural and anthropogenic impacts on environmental changes over the past 7500 years based on the multi-proxy study of shelf sediments in the northern South China Sea. *Quat. Sci. Rev.* **2018**, *197*, 35–48. [CrossRef]

7. Dou, Y.; Yang, S.; Liu, Z.; Clift, P.D.; Shi, X.; Yu, H.; Berne, S. Provenance discrimination of siliciclastic sediments in the middle Okinawa Trough since 30 ka: Constraints from rare earth element compositions. *Mar. Geol.* **2010**, *275*, 212–220. [CrossRef]

8. Abdullin, F.; Sole, J.; Solari, L.; Shchepetilnikova, V.; Meneses-Rocha, J.J.; Pavlinova, N.; Rodriguez-Trejo, A. Single-grain apatite geochemistry of Permian-Triassic granitoids and Mesozoic and Eocene sandstones from Chiapas, southeast Mexico: Implications for sediment provenance. *Int. Geol. Rev.* **2016**, *58*, 1132–1157. [CrossRef]

9. Boulay, S.; Colin, C.; Trentesaux, A.; Clain, S.; Liu, Z.; Lauer-Leredde, C. Sedimentary responses to the Pleistocene climatic variations recorded in the South China Sea. *Quat. Res.* **2007**, *68*, 162–172. [CrossRef]

10. Colin, C.; Siani, G.; Sicre, M.A.; Liu, Z. Impact of the East Asian monsoon rainfall changes on the erosion of the Mekong River basin over the past 25,000 yr. *Mar. Geol.* **2010**, *271*, 84–92. [CrossRef]

11. Wan, S.; Clift, P.D.; Li, A.; Yu, Z.; Li, T.; Hu, D. Tectonic and climatic controls on long-term silicate weathering in Asia since 5 Ma. *Geophys. Res. Lett.* **2012**, *39*, L15611. [CrossRef]

12. Wan, S.; Clift, P.D.; Zhao, D.; Hovius, N.; Munhoven, G.; France-Lanord, C.; Wang, Y.; Xiong, Z.; Jie, H.; Yu, Z. Enhanced silicate weathering of tropical shelf sediments exposed during glacial lowstands: a sink for atmospheric CO_2. *Geochim. Cosmochim. Acta* **2017**, *200*, 123–144. [CrossRef]

13. Liu, Z.; Zhao, Y.; Colin, C.; Stattegger, K.; Wiesner, M.G.; Huh, C.A.; Zhang, Y.; Li, X.; Sompongchaiyakul, P.; You, C.F. Source-to-sink transport processes of fluvial sediments in the South China Sea. *Earth Sci. Rev.* **2016**, *153*, 238–273. [CrossRef]

14. Morton, A.C.; Hallsworth, C. Identifying provenance-specific features of detrital heavy mineral assemblages in sandstones. *Sediment. Geol.* **1994**, *90*, 241–256. [CrossRef]

15. Morton, A.C.; Hallsworth, C.R. Processes controlling the composition of heavy mineral assemblages in sandstones. *Sediment. Geol.* **1999**, *124*, 3–29. [CrossRef]

16. Svendsen, J.B.; Hartley, N.R. Synthetic heavy mineral stratigraphy: Applications and limitations. *Mar. Pet. Geol.* **2002**, *19*, 389–405. [CrossRef]

17. Morton, A.C.; Whitham, A.G.; Fanning, C.M. Provenance of Late Cretaceous to Paleocene submarine fan sandstones in the Norwegian Sea: Integration of heavy mineral, mineral chemical and zircon age data. *Sediment. Geol.* **2005**, *182*, 3–28. [CrossRef]

18. Yang, S.; Wang, Z.; Guo, Y.; Li, C.; Cai, J. Heavy mineral compositions of the Changjiang (Yangtze River) sediments and their provenance-tracing implication. *J. Asian Earth Sci.* **2009**, *35*, 56–65. [CrossRef]

19. Dill, H.G. a review of heavy minerals in clastic sediments with case studies from the alluvial-fan through the nearshore-marine environments. *Earth Sci. Rev.* **1998**, *45*, 103–132. [CrossRef]

20. Belousova, E.A.; Griffin, W.L.; O'Reilly, S.Y.; Fisher, N.I. Apatite as an indicator mineral for mineral exploration: Trace-element compositions and their relationship to host rock type. *J. Geochem. Explor.* **2002**, *76*, 45–69. [CrossRef]

21. Morton, A.; Yaxley, G. Detrital apatite geochemistry and its application in provenance studies. *Spec. Pap. Geol. Soc. Am.* **2007**, *420*, 319–344.

22. Jafarzadeh, M.; Harami, R.M.; Friis, H.; Amini, A.; Mahboubi, A.; Lenaz, D. Provenance of the Oligocene-Miocene Zivah Formation, NW Iran, assessed using heavy mineral assemblage and detrital clinopyroxene and detrital apatite analyses. *J. Afr. Earth. Sci.* **2014**, *89*, 56–71. [CrossRef]

23. Gillespie, J.; Glorie, S.; Khudoley, A.; Collins, A.S. Detrital apatite U-Pb and trace element analysis as a provenance tool: Insights from the Yenisey Ridge (Siberia). *Lithos* **2018**, *314*, 140–155. [CrossRef]

24. Piccoli, P.M.; Candela, P.A. Apatite in igneous systems. *Rev. Mineral. Geochem.* **2002**, *48*, 255–292. [CrossRef]

25. Bouch, J.E.; Hole, M.J.; Trewin, N.H.; Chenery, S.; Morton, A.C. Authigenic apatite in a fluvial sandstone sequence: Evidence for rare-earth element mobility during diagenesis and a tool for diagenetic correlation. *J. Sediment. Res.* **2002**, *72*, 59–67. [CrossRef]

26. Spear, F.S.; Pyle, J.M. Apatite, monazite, and xenotime in metamorphic rocks. *Rev. Mineral. Geochem.* **2002**, *48*, 293–335. [CrossRef]

27. Nash, W.P. Phosphate Minerals. In *Phosphate Minerals in Terrestrial Igneous and Metamorphic Rocks*; Nriagu, J.O., Moore, P.B., Eds.; Springer: Berlin/Heidelberg, Germany, 1984; pp. 215–241.

28. Sha, L.K.; Chappell, B.W. Apatite chemical composition, determined by electron microprobe and laser-ablation inductively coupled plasma mass spectrometry, as a probe into granite petrogenesis. *Geochim. Cosmochim. Acta* **1999**, *63*, 3861–3881. [CrossRef]

29. Chu, M.-F.; Wang, K.-L.; Griffin, W.L.; Chung, S.-L.; O'Reilly, S.Y.; Pearson, N.J.; Iizuka, Y. Apatite Composition: Tracing Petrogenetic Processes in Transhimalayan Granitoids. *J. Petrol.* **2009**, *50*, 1829–1855. [CrossRef]

30. Katayama, H.; Watanabe, Y. The Huanghe and Changjiang contribution to seasonal variability in terrigenous particulate load to the Okinawa Trough. *Deep-Sea Res. Part Ii-Top. Stud. Oceanogr.* **2003**, *50*, 475–485. [CrossRef]

31. Dou, Y.; Yang, S.; Liu, Z.; Shi, X.; Li, J.; Yu, H.; Berne, S. Sr-Nd isotopic constraints on terrigenous sediment provenances and Kuroshio Current variability in the Okinawa Trough during the late Quaternary. *Palaeogeogr. Palaeoclimatol. Palaeoecol.* **2012**, *365*, 38–47. [CrossRef]

32. Li, T.; Xu, Z.; Lim, D.; Chang, F.; Wan, S.; Jung, H.; Choi, J. Sr-Nd isotopic constraints on detrital sediment provenance and paleoenvironmental change in the northern Okinawa Trough during the late Quaternary. *Palaeogeogr. Palaeoclimatol. Palaeoecol.* **2015**, *430*, 74–84. [CrossRef]

33. Liu, J.; Zhu, R.; Li, T.; Li, A.; Li, J. Sediment-magnetic signature of the mid-Holocene paleoenvironmental change in the central Okinawa Trough. *Mar. Geol.* **2007**, *239*, 19–31. [CrossRef]

34. Diekmann, B.; Hofmann, J.; Henrich, R.; Fuetterer, D.K.; Roehl, U.; Wei, K.-Y. Detrital sediment supply in the southern Okinawa Trough and its relation to sea-level and Kuroshio dynamics during the late Quaternary. *Mar. Geol.* **2008**, *255*, 83–95. [CrossRef]

35. Bentahila, Y.; Ben Othman, D.; Luck, J.-M. Strontium, lead and zinc isotopes in marine cores as tracers of sedimentary provenance: a case study around Taiwan orogen. *Chem. Geol.* **2008**, *248*, 62–82. [CrossRef]

36. Zheng, X.; Li, A.; Wan, S.; Jiang, F.; Kao, S.J.; Johnson, C. ITCZ and ENSO pacing on East Asian winter monsoon variation during the Holocene: Sedimentological evidence from the Okinawa Trough. *J. Geophys. Res.-Ocean.* **2014**, *119*, 4410–4429. [CrossRef]

37. Wang, J.; Li, A.; Xu, K.; Zheng, X.; Huang, J. Clay mineral and grain size studies of sediment provenances and paleoenvironment evolution in the middle Okinawa Trough since 17 ka. *Mar. Geol.* **2015**, *366*, 49–61. [CrossRef]

38. Zhao, D.; Wan, S.; Toucanne, S.; Clift, P.D.; Tada, R.; Revillon, S.; Kubota, Y.; Zheng, X.; Yu, Z.; Huang, J.; et al. Distinct control mechanism of fine-grained sediments from Yellow River and Kyushu supply in the northern Okinawa Trough since the last glacial. *Geochem. Geophys. Geosyst.* **2017**, *18*, 2949–2969. [CrossRef]

39. Zhao, D.; Wan, S.; Clift, P.D.; Tada, R.; Huang, J.; Yin, X.; Liao, R.; Shen, X.; Shi, X.; Li, A. Provenance, sea-level and monsoon climate controls on silicate weathering of Yellow River sediment in the northern Okinawa Trough during late last glaciation. *Palaeogeogr. Palaeoclimatol. Palaeoecol.* **2018**, *490*, 227–239. [CrossRef]

40. Ujiie, H.; Ujiie, Y. Late Quaternary course changes of the Kuroshio Current in the Ryukyu Arc region, northwestern Pacific Ocean. *Mar. Micropaleontol.* **1999**, *37*, 23–40. [CrossRef]

41. Xu, X.D.; Oda, M. Surface-water evolution of the eastern East China Sea during the last 36,000 years. *Mar. Geol.* **1999**, *156*, 285–304. [CrossRef]

42. Jian, Z.M.; Wang, P.X.; Saito, Y.; Wang, J.L.; Pflaumann, U.; Oba, T.; Cheng, X.R. Holocene variability of the Kuroshio Current in the Okinawa Trough, northwestern Pacific Ocean. *Earth Planet. Sci. Lett.* **2000**, *184*, 305–319. [CrossRef]

43. Chung, Y.; Chang, W.C. Pb-210 fluxes and sedimentation rates on the lower continental slope between Taiwan and the South Okinawa Trough. *Cont. Shelf Res.* **1995**, *15*, 149–164. [CrossRef]

44. Milliman, J.D.; Farnsworth, K.L. *River Discharge to the Coastal Ocean: a Global Synthesis*; Cambridge University Press: Cambridge, UK, 2011; p. 305. ISBN 978-0-521-87987-3.

45. Huang, C.-Y.; Yen, Y.; Zhao, Q.; Lin, C.-T. Cenozoic stratigraphy of Taiwan: Window into rifting, stratigraphy and paleoceanography of South China Sea. *Chin. Sci. Bull.* **2012**, *57*, 3130–3149. [CrossRef]

46. Horng, C.-S.; Huh, C.-A.; Chen, K.-H.; Lin, C.-H.; Shea, K.-S.; Hsiung, K.-H. Pyrrhotite as a tracer for denudation of the Taiwan orogen. *Geochem. Geophys. Geosyst.* **2012**, *13*, Q08Z47. [CrossRef]

47. Li, C.-S.; Shi, X.-F.; Kao, S.-J.; Liu, Y.-G.; Lyu, H.-H.; Zou, J.-J.; Liu, S.-F.; Qiao, S.-Q. Rare earth elements in fine-grained sediments of major rivers from the high-standing island of Taiwan. *J. Asian Earth Sci.* **2013**, *69*, 39–47. [CrossRef]

48. Lan, Q.; Yan, Y.; Huang, C.-Y.; Clift, P.D.; Li, X.; Chen, W.; Zhang, X.; Yu, M. Tectonics, topography, and river system transition in East Tibet: Insights from the sedimentary record in Taiwan. *Geochem. Geophys. Geosyst.* **2014**, *15*, 3658–3674. [CrossRef]

49. Zhang, K.; Xu, W.; Chen, S.; Mao, J.; Fan, D. Geological survey in Taiwan area. *Geol. Fujian* **2017**, *36*, 79–93. (In Chinese with English Abstract).

50. Geng, W.; Zhang, X.; Huang, L.; Wei, H.; Huang, C. Regional geological features and neotectonic movement of Taiwan inland and offshore areas. *Mar. Geol. Quat. Geol.* **2014**, *34*, 73–82. (In Chinese with English Abstract).

51. Dadson, S.J.; Hovius, N.; Chen, H.G.; Dade, W.B.; Hsieh, M.L.; Willett, S.D.; Hu, J.C.; Horng, M.J.; Chen, M.C.; Stark, C.P.; et al. Links between erosion, runoff variability and seismicity in the Taiwan orogen. *Nature* **2003**, *426*, 648–651. [CrossRef]

52. Kao, S.J.; Lee, T.Y.; Milliman, J.D. Calculating highly fluctuated suspended sediment fluxes from mountainous rivers in Taiwan. *Terr. Atmos. Ocean. Sci.* **2005**, *16*, 653–675. [CrossRef]

53. Wan, S.; Li, A.; Clift, P.D.; Wu, S.; Xu, K.; Li, T. Increased contribution of terrigenous supply from Taiwan to the northern South China Sea since 3 Ma. *Mar. Geol.* **2010**, *278*, 115–121. [CrossRef]

54. Kao, S.J.; Liu, K.K. Estimating the suspended sediment load by using the historical hydrometric record from the Lanyang-Hsi watershed. *Terr. Atmos. Ocean. Sci.* **2001**, *12*, 401–414. [CrossRef]

55. Jeng, W.L.; Lin, S.; Kao, S.J. Distribution of terrigenous lipids in marine sediments off northeastern Taiwan. *Deep-Sea Res. Part Ii-Top. Stud. Oceanogr.* **2003**, *50*, 1179–1201. [CrossRef]

56. Kao, S.J.; Lin, F.J.; Liu, K.K. Organic carbon and nitrogen contents and their isotopic compositions in surficial sediments from the East China Sea shelf and the southern Okinawa Trough. *Deep-Sea Res. Part II Top. Stud. Oceanogr.* **2003**, *50*, 1203–1217. [CrossRef]

57. Hsu, S.C.; Lin, F.J.; Jeng, W.L.; Chung, Y.C.; Shaw, L.M.; Hung, K.W. Observed sediment fluxes in the southwesternmost Okinawa Trough enhanced by episodic events: Flood runoff from Taiwan rivers and large earthquakes. *Deep-Sea Res. Part I-Oceanogr. Res. Pap.* **2004**, *51*, 979–997. [CrossRef]

58. Liu, K.K.; Peng, T.H.; Shaw, P.T.; Shiah, F.K. Circulation and biogeochemical processes in the East China Sea and the vicinity of Taiwan: An overview and a brief synthesis. *Deep-Sea Res. Part Ii-Top. Stud. Oceanogr.* **2003**, *50*, 1055–1064. [CrossRef]

59. Hu, S.; Zeng, Z.; Fang, X.; Qi, H.; Yin, X.; Chen, Z.; Li, X.; Zhu, B. Increased contribution of terrigenous supply from Taiwan to the southern Okinawa Trough over the past 3000 years. *Sediment. Geol.*. Under Revision.

60. Blaauw, M.; Andres Christen, J. Flexible Paleoclimate Age-Depth Models Using an Autoregressive Gamma Process. *Bayesian Anal.* **2011**, *6*, 457–474.

61. Zong, K.; Klemd, R.; Yuan, Y.; He, Z.; Guo, J.; Shi, X.; Liu, Y.; Hu, Z.; Zhang, Z. The assembly of Rodinia: The correlation of early Neoproterozoic (ca. 900 Ma) high-grade metamorphism and continental arc formation in the southern Beishan Orogen, southern Central Asian Orogenic Belt (CAOB). *Precambrian Res.* **2017**, *290*, 32–48. [CrossRef]

62. Hu, Z.; Zhang, W.; Liu, Y.; Gao, S.; Li, M.; Zong, K.; Chen, H.; Hu, S. "Wave" Signal-Smoothing and Mercury-Removing Device for Laser Ablation Quadrupole and Multiple Collector ICPMS Analysis: Application to Lead Isotope Analysis. *Anal. Chem.* **2015**, *87*, 1152–1157. [CrossRef]

63. Liu, Y.; Hu, Z.; Gao, S.; Guenther, D.; Xu, J.; Gao, C.; Chen, H. In situ analysis of major and trace elements of anhydrous minerals by LA-ICP-MS without applying an internal standard. *Chem. Geol.* **2008**, *257*, 34–43. [CrossRef]

64. Liao, J.; Sun, X.; Li, D.; Sa, R.; Lu, Y.; Lin, Z.; Xu, L.; Zhan, R.; Pan, Y.; Xu, H. New insights into nanostructure and geochemistry of bioapatite in REE-rich deep-sea sediments: LA-ICP-MS, TEM, and Z-contrast imaging studies. *Chem. Geol.* **2019**, *512*, 58–68. [CrossRef]

65. Fleischer, M.; Altschuler, Z.S. The lanthanides and yttrium in minerals of the apatite group—An analysis of the available data. *Neues Jahrb. Fur Mineral.-Mon.* **1986**, *10*, 467–480.

66. Dill, H.G. Can REE patterns and U-Th variations be used as a tool to determine the origin of apatite in clastic rocks? *Sediment. Geol.* **1994**, *92*, 175–196. [CrossRef]

67. Qiu, J.; Zhang, X.; Hu, J.; Li, Z. In situ LA-ICP-MS analyses of apatites from carbonatites in western Shandong province: Implications for petrogenesis. *Acta Petrol. Sin.* **2009**, *25*, 2855–2865.

68. Guo, S.; Ye, K.; Wu, T.F.; Chen, Y.; Yang, Y.H.; Zhang, L.M.; Liu, J.B.; Mao, Q.; Ma, Y.G. a potential method to confirm the previous existence of lawsonite in eclogite: The mass imbalance of Sr and LREEs in multistage epidote (Ganghe, Dabie UHP terrane). *J. Metamorph. Geol.* **2013**, *31*, 415–435. [CrossRef]

69. Wen, D.-R.; Chung, S.-L.; Song, B.; Iizuka, Y.; Yang, H.-J.; Ji, J.; Liu, D.; Gallet, S. Late Cretaceous Gangdese intrusions of adakitic geochemical characteristics, SE Tibet: Petrogenesis and tectonic implications. *Lithos* **2008**, *105*, 1–11. [CrossRef]

70. Henrichs, I.A.; O'Sullivan, G.; Chew, D.M.; Mark, C.; Babechuk, M.G.; McKenna, C.; Emo, R. The trace element and U-Pb systematics of metamorphic apatite. *Chem. Geol.* **2018**, *483*, 218–238. [CrossRef]

71. Bingen, B.; Demaiffe, D.; Hertogen, J. Redistribution of rare earth elements, thorium, and uranium over accessory minerals in the course of amphibolite to granulite facies metamorphism: The role of apatite and monazite in orthogneisses from southwestern Norway. *Geochim. Cosmochim. Acta* **1996**, *60*, 1341–1354. [CrossRef]

72. Bea, F.; Montero, P. Behavior of accessory phases and redistribution of Zr, REE, Y, Th, and U during metamorphism and partial melting of metapelites in the lower crust: An example from the Kinzigite Formation of Ivrea-Verbano, NW Italy. *Geochim. Cosmochim. Acta* **1999**, *63*, 1133–1153. [CrossRef]

73. Taylor, S.R.; Mclennan, S.M. The continental crust: Its composition and evolution. *J. Geol.* **1985**, *94*, 632–633.

74. Zhao, Z.; Bao, Z.; Qiao, Y. a peculiar composite M-and W-type REE tetrad effect: Evidence from the Shuiquangou alkaline syenite complex, Hebei Province. *Chin. Sci. Bull.* **2010**, *55*, 1474–1488. (In Chinese with English Abstract). [CrossRef]

75. Frietsch, R.; Perdahl, J.A. Rare earth elements in apatite and magnetite in Kiruna-type iron ores and some other iron ore types. *Ore Geol. Rev.* **1995**, *9*, 489–510. [CrossRef]

76. Chen, Z.; Zeng, Z.; Wang, X.; Yin, X.; Chen, S.; Guo, K.; Lai, Z.; Zhang, Y.; Ma, Y.; Qi, H.; et al. U-Th/He dating and chemical compositions of apatite in the dacite from the southwestern Okinawa Trough: Implications for petrogenesis. *J. Asian Earth Sci.* **2018**, *161*, 1–13. [CrossRef]

77. Nutman, A.P. Apatite recrystallisation during prograde metamorphism, Cooma, southeast Australia: Implications for using an apatite-graphite association as a biotracer in ancient metasedimentary rocks. *Aust. J. Earth Sci.* **2007**, *54*, 1023–1032. [CrossRef]

78. Spandler, C.; Hermann, J.; Arculus, R.; Mavrogenes, J. Redistribution of trace elements during prograde metamorphism from lawsonite blueschist to eclogite facies; implications for deep subduction-zone processes. *Contrib. Mineral. Petrol.* **2003**, *146*, 205–222. [CrossRef]

79. Chen, Z.; Zeng, L.; Meng, L. Mineralogy and trace elemental geochemistry of apatite in Sulu eclogites. *Acta Petrol. Sin.* **2009**, *25*, 1663–1677.

80. O'Sullivan, G.J.; Chew, D.M.; Morton, A.C.; Mark, C.; Henrichs, I.A. An Integrated Apatite Geochronology and Geochemistry Tool for Sedimentary Provenance Analysis. *Geochem. Geophys. Geosyst.* **2018**, *19*, 1309–1326. [CrossRef]

81. Oksanen, J.; Blanchet, F.G.; Friendly, M.; Kindt, R.; Legendre, P.; McGlinn, D.; Minchin, P.R.; O'Hara, R.B.; Simpson, G.L.; Solymos, P.; et al. *Vegan: Community Ecology Package, R package Version 2.5-6*; Jari Oksanen: Helsinki, Finland, 2019.

82. Tang, M.; Wang, X.L.; Xu, X.S.; Zhu, C.; Cheng, T.; Yu, Y. Neoproterozoic subducted materials in the generation of Mesozoic Luzong volcanic rocks: Evidence from apatite geochemistry and Hf–Nd isotopic decoupling. *Gondwana Res.* **2012**, *21*, 266–280. [CrossRef]

83. Xiang, R.; Sun, Y.; Li, T.; Oppo, D.W.; Chen, M.; Zheng, F. Paleoenvironmental change in the middle Okinawa Trough since the last deglaciation: Evidence from the sedimentation rate and planktonic foraminiferal record. *Palaeogeogr. Palaeoclimatol. Palaeoecol.* **2007**, *243*, 378–393. [CrossRef]

84. Li, T.; Liu, Z.; Hall, M.A.; Berne, S.; Saito, Y.; Cang, S.; Cheng, Z. Heinrich Event imprints in the Okinawa Trough: Evidence from oxygen isotope and planktonic Foraminifera. *Palaeogeogr. Palaeoclimatol. Palaeoecol.* **2001**, *176*, 133–146. [CrossRef]

85. Lambeck, K.; Yokoyama, Y.; Purcell, T. Into and out of the Last Glacial Maximum: Sea-level change during Oxygen Isotope Stages 3 and 2. *Quat. Sci. Rev.* **2002**, *21*, 343–360. [CrossRef]

86. Wang, Y.; Cheng, H.; Edwards, R.L.; He, Y.; Kong, X.; An, Z.; Wu, J.; Kelly, M.J.; Dykoski, C.A.; Li, X. The Holocene Asian monsoon: Links to solar changes and North Atlantic climate. *Science* **2005**, *308*, 854–857. [CrossRef] [PubMed]

87. Cullers, R.L. The controls on the major and trace element variation of shales, siltstones, and sandstones of Pennsylvanian-Permian age from uplifted continental blocks in Colorado to platform sediment in Kansas, USA. *Geochim. Cosmochim. Acta* **1994**, *58*, 4955–4972. [CrossRef]

88. Hubert, J.F. a Zircon-Tourmaline-Rutile Maturity Index and the Interdependence of the Composition of Heavy Mineral Assemblages with the Gross Composition and Texture of Sandstones. *J. Sediment. Petrol.* **1962**, *32*, 440–450.

89. Li, C.; Shi, X.; Kao, S.; Chen, M.; Liu, Y.; Fang, X.; Lu, H.; Zou, J.; Liu, S.; Qiao, S. Clay mineral composition and their sources for the fluvial sediments of Taiwanese rivers. *Chin. Sci. Bull.* **2012**, *57*, 673–681. [CrossRef]